Investigation of the effect of surcharge on behavior of soil slopes

Mohammad Mahdi Aminpour[*1], Mohammad Maleki[1a] and Ali Ghanbari[2b]

[1]*Department of Civil Engineering, Bu-Ali Sina University, Hamedan, I.R. Iran*
[2]*Faculty of Engineering, Kharazmi University, No. 49 Mofatteh Ave. Tehran, I.R. Iran*

Abstract.   By increase in the population and consequently constructions, new structures may be built in vicinity of the soil slopes. Such structures can be regarded as an extra surcharge on the slopes. The intensity and location of the surcharge affects the displacements of the slopes. Few researchers have studied the effect of surcharge on displacements of soil slopes. In this research, using limit analysis method and upper bound theory with non-associated flow rule, displacements of soil slopes in vicinity of a surcharge has been estimated. The authors have improved the technique previously proposed by them and a new formulation is suggested for calculating the permanent displacements of the soil slope in presence of a surcharge for two failure modes, rotational and transitional. A comparison has also been made between the two mentioned modes for various conditions of surcharge and slope. The conditions resulting in the rotational mode to be more critical than the transitional mode have been investigated. Also, the effects of surcharge's intensity, location of surcharge as well as the soil properties have been investigated.

Keywords: surcharge; soil slopes; displacement; limit analysis

1. Introduction

There have been various analytical, numerical and experimental studies on displacements of reinforced slopes. In analytical studies, the kinematic theorem of limit analysis presented by Ausilio *et al.* (2000), Michalowski and You (2000) and Michalowski (2007) that calculated the yield acceleration and displacement of reinforced soil slopes. Askari and Farzaneh (2003) calculated seismic bearing capacity of shallow foundations near slopes. Mojallal and Ghanbari (2012) and Mojallal *et al.* (2012) calculated the displacement of gravity retaining walls and reinforced soil walls. Aminpoor and Ghanbari (2014) studied the displacements of retaining walls in vicinity of a surcharge for two conditions of sliding and overturning. They proposed design charts for this purpose. Yu *et al.* (2014) studied the pullout capacity for plate anchors in sandy slopes. Zhang *et al.* (2016) studied 3D rock slope stability with non-linear failure criterion. Fei *et al.* (2016) investigated the effect of the vertical acceleration on the safety of three-dimensional

---

∗Corresponding author, Ph.D. Student, E-mail: Aminpour.geoeng@gmail.com
[a]Associate Professor, E-mail: Maleki@basu.ac.ir
[b]Professor, E-mail: Ghanbari@khu.ac.ir

slopes. In this regard, they used a kinematically admissible rotational failure mechanism for homogeneous slopes. Cai and Bathurst (1996) and Huang and Wang (2005), Huang and Wu (2006, 2007) and Huang and Wu (2009) used the limit equilibrium technique to calculate the seismic displacement of geosynthetic-reinforced soil walls. Varzaghani and Ghanbari calculated dynamic displacement of foundations adjacent to slope using the spring dashpot method. Ghanbari and Taheri (2012) and Ghanbari *et al.* (2013) obtained active earth pressure and seismic displacement for a reinforced slope with a linear surcharge using the horizontal slices method. Caltabiano *et al.* (2005) proposed a procedure for seismic design of retaining walls accounting for the actual failure mechanism mobilized in limit equilibrium conditions. Caltabiano *et al.* (2012) calculated the angle of failure and critical acceleration as well as coefficient of active pressure to retaining walls in the presence of various surcharges for static and seismic conditions.

Among the experimental studies, following works can be mentioned: El-Emam and Bathurst (2005, 2007), Huang *et al.* (2008), Madhavi Latha and Murali Krishna (2008), Tatsuoka *et al.* (2009), Krishna and Latha (2009), Yang *et al.* (2009), Bathurst *et al.* (2009), Huang and Luo (2010), Huang *et al.* (2011), Bathurst *et al.* (2012) and Srilatha *et al.* (2013). Numerical studies include those by Liu (2009), Lee *et al.* (2010), Liu and Wang (2011) and Liang *et al.* (2017).

In the present research, using limit analysis method, the yield acceleration and displacements of soil slopes in presence of a surcharge (ex. a building) has been studied. Two failure modes, rotational and transitional, have been considered in this research. The two failure modes have been compared and considering the surcharge, the cases in which the rotational failure mode would be more critical than the transitional mode have been investigated. Finally, the effect of factors such as intensity and location of surcharge and properties of the soil slope have been evaluated.

2. Theorems for non-associated flow rules

In the investigation of non-associated flow rule, Sloan (2013) discussed that the flow rule will not have a major influence on the failure load for frictional soils unless the problem is heavily constrained in a kinematic manner. A precise definition of the degree of kinematic constraint is elusive, but many geotechnical failure modes are not heavily constrained, since they involve a freely deforming ground surface and a semi-infinite domain. For these cases, Davis (1968) conjectured that it is reasonable to suppose that the bound theorems will give well estimates of the true failure limit load (Sloan 2013). In addition, by examining the failure mechanism on slip-lines for a non-associated Mohr Coulomb material, he established that the shear and normal stress are related by

$$\tau = \sigma_n \tan \phi^* + c^* \tag{1}$$

Where c^* and ϕ^* are 'reduced' strength parameters, defined by

$$\left.\begin{array}{l} c^* = \beta c \\ \tan \phi^* = \beta \tan \phi \end{array}\right\} \quad \beta = \frac{\cos\psi \cos\phi}{1 - \sin\psi \sin\phi} \tag{2}$$

c is the cohesion, ϕ is the internal friction angle and ψ is the dilation angle. The use of these reduced strengths provides a practical means for non-associated flow rule in limit analysis (Sloan 2013, Michalowski 2007).
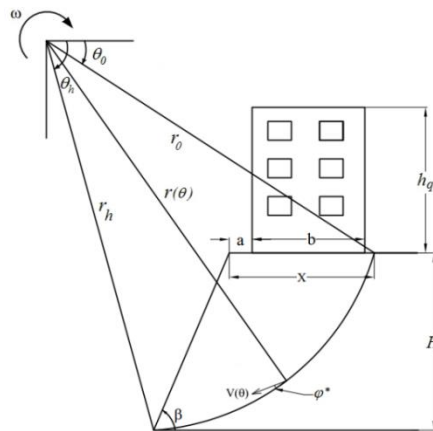
Fig. 1 Rotational failure mechanism and the excess surcharge due to the building next to the slope
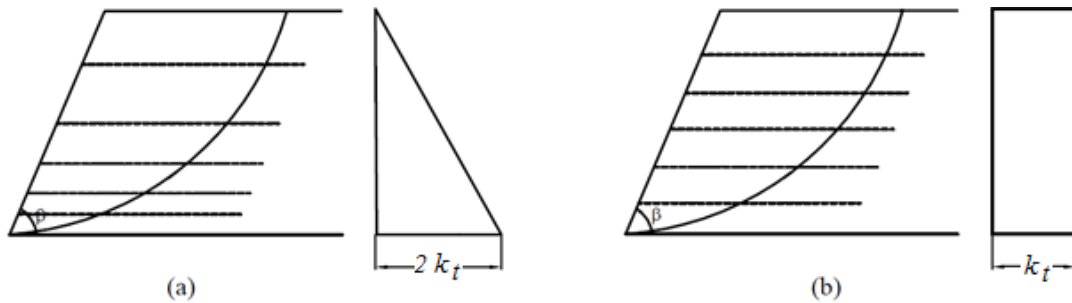
Fig. 2 Schematic internal force distribution in the height of the slope (a) uniform distribution of forces and (b) rectangular distribution of forces

3. Studying the rotational failure mechanism (log-spiral)

A soil slope with the internal friction angle of ϕ and cohesion of c is located next to a building (Fig. 1). This slope undergoes the horizontal and vertical seismic accelerations of k_h and k_v, respectively. In this analysis it is assumed that the failure wedge is rigid and the inertial force of earthquake is applied pseudo-statically. This slope can fail in either of two mechanisms, log-spiral rotational mechanism and planar transitional mechanism. The force of reinforcements is introduced with the k_t parameter defined as following

$$k_t = \frac{\sum_{i=1}^{n} T_i}{H} \tag{3}$$

In Eq. (3), n is the number of reinforcing layers, T_i is the force of each layer of reinforcements (per unit width) and H is the height of the slope.

3.1 Calculation of the yield acceleration in log-spiral rotational failure mechanism

For the rotational failure case as illustrated in Fig. 1, the reinforced soil wedge rotates around

the point O with the angular velocity ω. In this figure, X is the width of the failure wedge, a is the distance of surcharge from the edge of the slope, b is the width of the surcharge and h_q is the height of the surcharge. The formula for the log-spiral failure surface can be expressed by Eq. (4). In this equation, $r(\theta)$ is the radius as a function of the arbitrary angle θ and $V(\theta)$ is the incipient velocity as a function of $r(\theta)$.

$$r(\theta) = r_0 \exp\left[(\theta - \theta_0)\tan \varphi^*\right] \tag{4}$$

It has to be noted that the failure surface moves along the heel of the slope and can be located either in front of or behind the reinforced area.

In order to calculate the rate of internal work due to cohesion, an increment of the energy distributed in an element with the size of $rd\theta/\cos\varphi$ has been considered. The work done by the cohesion is obtained integrating the entire failure surface (Chen 2008).

$$\dot{D}_c = \int_{\theta_0}^{\theta_h} c^* \left(V \cos\varphi^*\right)\frac{r\,d\theta}{\cos\varphi^*} = \frac{1}{2}c^* r_0^2 \frac{1}{\tan\varphi^*}\left\{\exp\left[2(\theta_h - \theta_0)\tan\varphi^*\right] - 1\right\}\omega \tag{5}$$

The rate of work due to the reinforcements would depend on their distribution in the height of the slope. The reinforcements with the same strengths have two types of triangular and uniform distributions in the height with regard to their distance (Fig. 2). The rate of internal work for the two cases of triangular and uniform distribution can be obtained from Eqs. (6) and (7), respectively (Michalowski 1998).

$$\dot{D}_t = \frac{1}{3}k_t\,\omega r_0^2 \left(2\sin^2\theta_h \exp\left[2(\theta_h - \theta_0)\tan\varphi^*\right] - \sin\theta_0 \sin\theta_h \exp\left[(\theta_h - \theta_0)\tan\varphi^*\right] - \sin^2\theta_0\right) \tag{6}$$

$$\dot{D}_t = \frac{1}{2}k_t\,\omega r_0^2 \left(\sin^2\theta_h \exp\left[2(\theta_h - \theta_0)\tan\varphi^*\right] - \sin^2\theta_0\right) \tag{7}$$

The rate of work done by body forces can be obtained from Eq. (8) regardless of the location of the surcharge. In this equation, the functions f_1 to f_6 are dependent on θ_0, θ_h, φ, and β parameter. These functions have been introduced by other researchers (Crespellani *et al.* 1998, Michalowski 1998) and are summarized in the appendix. In this paper, φ^* must be used instead of φ.

$$\dot{W} = \gamma r_0^3\,\omega\left(f_1 - f_2 - f_3\right)\left(1 - k_v\right) + k_h\,\gamma r_0^3\,\omega\left(f_4 - f_5 - f_6\right) \tag{8}$$

In order to calculate the minimum rate of external work due to the surcharge, three different cases of surcharge's location have been considered as following:
  1. Case 1: The surcharge is completely located within the failure wedge
  2. Case 2: The surcharge is partially located within the failure wedge
  3. Case 3: The surcharge is completely located outside the failure wedge.
Considering the forces applied to the failure wedge and the length of their arms from the center of rotation, the rate of external work due to the surcharge for case 1 can be calculated by Eq. (9).

$$\dot{Q} = qb\left(1 - k_v\right)\left(r_0 \cos\theta_0 - X + a + \frac{b}{2}\right)\omega + k_h qb\left(r_0 \sin\theta_0 - \bar{h}_q\right)\omega \tag{9}$$

In this equation $\bar{h}_q$ is the height of the center of mass of the building (surcharge) and X is the

width of the failure wedge (Fig. 1). The rate of external work due to surcharge in case 2 is obtained from Eq. (10). It has to be noted that in case 3, since the surcharge is located outside the failure wedge, the rate of external work is zero.

$$\dot{Q} = q(X-a)(1-k_v)\left(r_0\cos\theta_0 - \frac{X-a}{2}\right)\omega + k_h q(X-a)(r_0\sin\theta_0 - \bar{h}_q)\omega \tag{10}$$

In the ordinary condition, the rate of the internal work is greater than external work. Assuming at the time of failure the ground's acceleration has reached the yield acceleration ($k_y = k_h$), the rates of internal and external work can be equaled.

$$\dot{D}_c + \dot{D}_t = \dot{W} + \dot{Q} \tag{11}$$

Solving Eq. (11), the coefficient of yield acceleration for the three cases of surcharge can be obtained from Eqs. (12)-(16). It has to be mentioned that the value of ω will be canceled out from the denominator and numerator of these equations. The parameter λ is the ratio of horizontal to vertical seismic accelerations.

In case 1

$$k_y = \frac{\dot{D}_c + \dot{D}_t - \gamma r_0^3\left(f_1 - f_2 - f_3\right)\omega - qb\left(r_0\cos\theta_0 - X + a + \frac{b}{2}\right)\omega}{\gamma r_0^3\left[(f_4 - f_5 - f_6) - \lambda(f_1 - f_2 - f_3)\right]\omega + qb\bar{A}\,\omega} \tag{12}$$

$$\bar{A} = \left(r_0\sin\theta_0 - \bar{h}_q\right) - \lambda\left(r_0\cos\theta_0 - X + a + \frac{b}{2}\right) \tag{13}$$

In case 2

$$k_y = \frac{\dot{D}_c + \dot{D}_t - \gamma r_0^3\left(f_1 - f_2 - f_3\right)\omega - q(X-a)\left(r_0\cos\theta_0 - \frac{X-a}{2}\right)\omega}{\gamma r_0^3\left[(f_4 - f_5 - f_6) - \lambda(f_1 - f_2 - f_3)\right]\omega + q(X-a)\bar{B}\,\omega} \tag{14}$$

$$\bar{B} = \left(r_0\sin\theta_0 - \bar{h}_q\right) - \lambda\left(r_0\cos\theta_0 - \frac{X-a}{2}\right) \tag{15}$$

In case 3

$$k_y = \frac{\dot{D}_c + \dot{D}_t - \gamma r_0^3\left(f_1 - f_2 - f_3\right)\omega}{\gamma r_0^3\left[(f_4 - f_5 - f_6) - \lambda(f_1 - f_2 - f_3)\right]\omega} \tag{16}$$

$$\frac{\partial k_y}{\partial\theta_0} = \frac{\partial k_y}{\partial\theta_h} = 0 \tag{17}$$

The yield acceleration is a function of two parameters θ_0 and θ_h. By minimizing the coefficient of yield acceleration, the lowest value of k_y, is obtained as the coefficient of yield acceleration. By solving the obtained equations and Eq. (17) simultaneously, the critical coefficient of yield

acceleration can be calculated.

Since the analytical solution of these equations would be very complicated, they have been solved by trial and error using a code. For this purpose, a code in any programing language can be used to determine the coefficient of yield acceleration.

3.2 Calculating the permanent displacement for log-spiral rotational failure mechanism

Once $k_h > k_y$, the slope starts rotating. The external forces applied to the failure wedge include the weight of failure wedge and surcharge as well as moment of inertia due to the weight of building and failure wedge (Fig. 3). In this figure W_{ABC} is the weight of failure wedge and I_q and I_{ABC} are the moment of inertia of the failure wedge and building, respectively. During the rotation, the failure wedge starts moving with $\ddot{\theta}$ acceleration. $\overline{h_q}$ is the center of mass of the building and the point at which the forces due to surcharge are being applied. The angle of acceleration vector with all points on the failure wedge is equal to the internal friction angle of the soil.

During the movement of the slope, the rate of work done by body forces including weight of the failure wedge and inertia forces in all the cases of surcharge's location have equal values and can be obtained from Eq. (18). The moment of inertia for the failure wedge around the rotation point, O, can be obtained from Eq. (19). Derivation of I_{ABC} is explained in the appendix.

$$\dot{W} = \gamma r_0^{\,3} \omega \left(f_1 - f_2 - f_3 \right)\left(1 - k_v \right) + k_h \gamma r_0^{\,3} \omega \left(f_4 - f_5 - f_6 \right) - I_{ABC} \ddot{\theta} \omega \tag{18}$$

$$I_{ABC} = I_{OBC} - I_{OAB} - I_{OAC} \tag{19}$$

The rate of external work due to surcharge during rotation of failure wedge varies depending on the location of surcharge. With regard to the fact that the rate of external work equals with the rate of internal work obtained from Eq. (11), the rate of work done by surcharge and acceleration of the slope during the rotation in case 1, can be obtained from Eqs. (20) and (22), respectively. I_q is the moment of inertia of the surcharge calculated from Eq. (21).
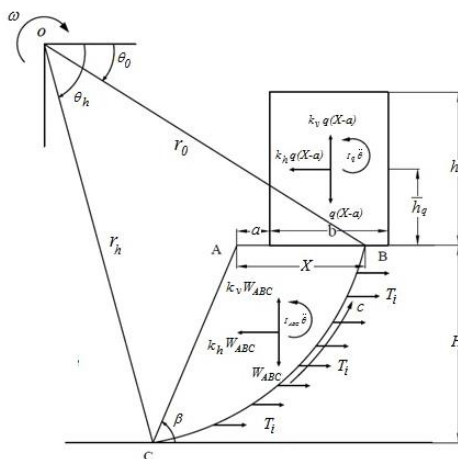
Fig. 3 Schematic illustration of the forces applied to the failure wedge during rotation
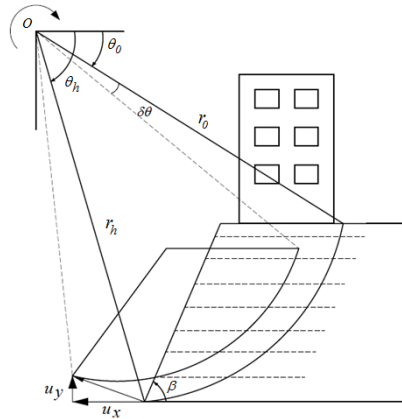
Fig. 4 Rotation of the failure wedge and its displacement at the end of the slope

ρ_q is the specific mass of surcharge. In order to simplify the equation, a part of it is shown by $c_{log-spiral}$. The value of $\overline{A}$ is equal to Eq. (13).

$$\dot{Q} = qb(1-k_v)\left(r_0 \cos\theta_0 - X + a + \frac{b}{2}\right)\omega + k_h qb(r_0 \sin\theta_0 - \overline{h}_q)\omega - I_q\ddot{\theta}\omega \tag{20}$$

$$I_q = \frac{\rho_q b h_q}{3}\left(h_q^2 + b^2\right) + b h_q \rho_q\left[(r_0 \sin\theta_0)^2 + (r_0\cos\theta_0 - X + a)^2\right] \tag{21}$$

$$\ddot{\theta} = (k_h - k_y)c_{log-spiral}$$
$$C_{log-spiral} = \frac{\gamma r_0^3\left[(f_4 - f_5 - f_6) - \lambda(f_1 - f_2 - f_3)\right] + qb\overline{A}}{I_{ABC} + I_q} \tag{22}$$

In case 2, the rate of work due to the external force of surcharge and rotational acceleration of slope can be obtained from Eqs. (20)-(22); the difference being that instead of b, $b_e = X - a$ has to be used. In case 3, the rate of work due to surcharge is zero and rotational acceleration of slope (in radian per second squared) is obtained from Eq. (23).

$$\ddot{\theta} = (k_h - k_y)C_{log-spiral}$$
$$C_{log-spiral} = \frac{\gamma r_0^3\left[(f_4 - f_5 - f_6) - \lambda(f_1 - f_2 - f_3)\right]}{I_{ABC}} \tag{23}$$

Finally, the angle of rotation of slope (in radian) can be obtained by twice integrating the acceleration

$$\theta = \int_t \int_t (k_h - k_y)C_{log-spiral} \ dt\,dt \tag{24}$$

The maximum horizontal movement of the failure wedge due to rotation occurs at the toe of the slope and with regard to Fig. 4, it can be calculated from Eq. (25).

$$u_x = r_h \sin \theta_h \int_t \int_t \ddot{\theta} \ dt \, dt = r_h \sin \theta_h \ C_{\log-spiral} \int_t \int_t (k_h - k_y) \ dt \, dt \qquad (25)$$

4. Studying the planar transitional mechanism

In this mechanism, the soil wedge acts as a rigid body transitioning with the velocity V (Fig. 5). The rate of internal work due to the cohesion and force of reinforcements can be obtained from Eqs. (24) and (25), respectively. In these equations α is the angle of failure wedge and X is the width of failure wedge equal to H (cot α−cot β).

$$\dot{D}_c = c^* \left(X^2 + \frac{H^2}{\sin^2 \beta} + \frac{2HX}{\tan \beta} \right) V \cos \varphi^* \qquad (26)$$

$$\dot{D}_t = \sum_{i=1}^{n} T_i \, V \cos(\alpha - \varphi^*) \qquad (27)$$

Rate of external work due to the weight of failure wedge is obtained from Eq. (28). In this equation W_{ABC} is equal to the weight of failure wedge as shown in Fig. 5.

$$\dot{W} = W_{ABC} V (1 - k_v) \sin(\alpha - \varphi^*) + k_h \, W_{ABC} V \cos(\alpha - \varphi^*) \qquad (28)$$

The rate of work due to surcharge is studied for three cases of surcharge's location and failure wedge, similar to the previous section. In the transitional mechanism, the force applied to the failure wedge and transitional velocity of the wedge are important. For the case where the surcharge is completely located within the failure wedge, the rate of work due to surcharge and coefficient of yield acceleration can be obtained from Eqs. (29) and (30), respectively. In this equation the velocity cancels out from the denominator and numerator.

$$\dot{Q} = qb(1 - k_v) V \sin(\alpha - \varphi^*) + k_h qb \cos(\alpha - \varphi^*) \qquad (29)$$

$$k_y = \frac{\dot{D}_c + \dot{D}_t - (W_{ABC} + qb) \sin(\alpha - \varphi^*) V}{(W_{ABC} + qb) \left[\cos(\alpha - \varphi^*) - \lambda \sin(\alpha - \varphi^*) \right] V} \qquad (30)$$
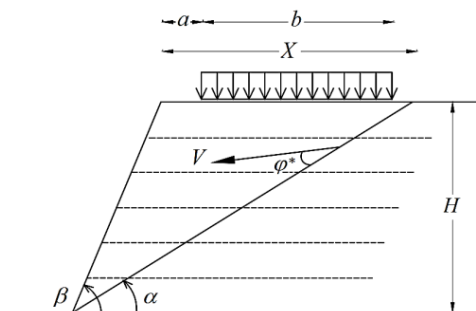
Fig. 5 Transitional failure mechanism and excess surcharge due to the building next to the slope
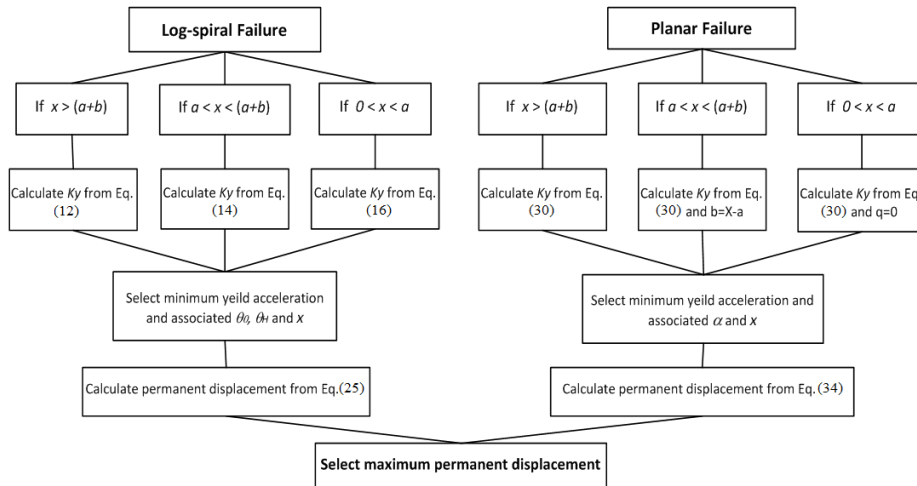
Fig. 6 The algorithm for obtaining the permanent displacement based on the suggested method


(a)

(b)
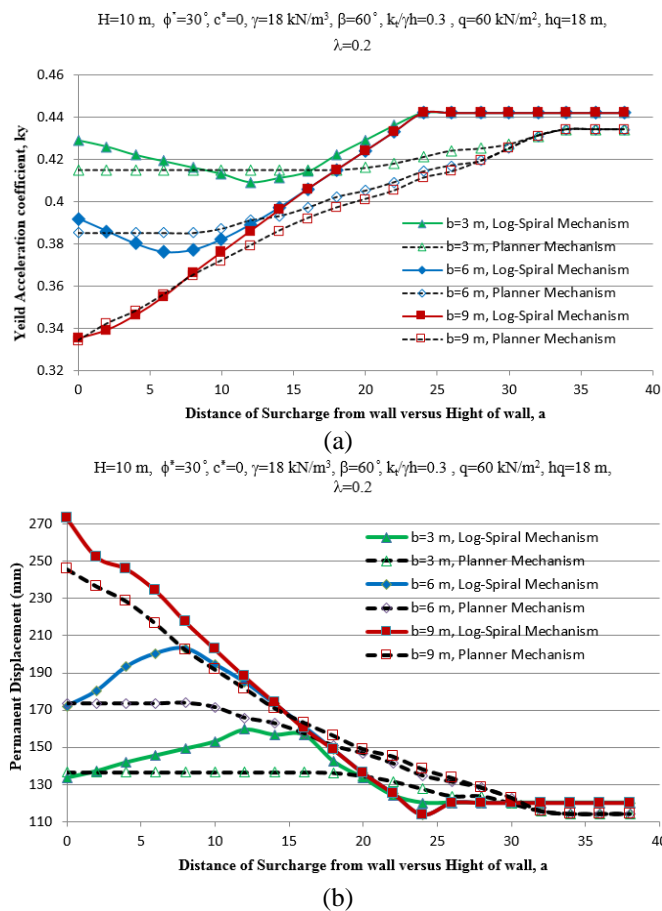
Fig. 7 Variations of (a) yield acceleration coefficient and (b) displacement of slope versus the distance of surcharge from the end of the slope for different widths of surcharge

In the case where only a part of the surcharge is within the failure wedge, the rate of work due to the surcharge and coefficient of yield acceleration can be obtained from Eqs. (29) and (30), respectively, the difference being b needs to be substituted with $X-a$. Also, for the case at which the surcharge is located completely outside the failure wedge, the rate of work due to the surcharge is zero and the coefficient of yield acceleration can be obtained from Eq. (30) by setting q equal to zero.

Once $k_h > k_y$, the slope starts sliding and the failure wedge moves with $\ddot{u}$ acceleration. The rate of work due to body forces during the sliding of the slope can be obtained from Eq. (31). In this equation m_{ABC} is the mass of the failure wedge.

$$\dot{W} = W_{ABC} V (1 - k_v) \sin(\alpha - \varphi^*) + k_h W_{ABC} V \cos(\alpha - \varphi^*) - m_{ABC} \ddot{u} V \tag{31}$$

The rate of external work due to surcharge during the slide of the slope for the case where surcharge is located completely within the failure wedge can be obtained from Eq. (32).

$$\dot{Q} = qb(1 - k_v)V \sin(\alpha - \varphi^*) + k_h qb \cos(\alpha - \varphi^*) - \frac{qb}{g} \ddot{u} V \tag{32}$$

For the case where only a part of surcharge is within the failure wedge, the rate of work due to the surcharge can be obtained from the previous equation substituting b with $X-a$. Also, for the case where surcharge is completely outside the failure wedge, the rate of the work of the surcharge is zero. By making the rate of internal and external works equal to each other, the acceleration and horizontal displacement of the slope can be obtained from Eqs. (33) and (34), respectively.

$$\ddot{u} = (k_h - k_y)g \left[\cos(\alpha - \varphi^*) - \lambda \sin(\alpha - \varphi^*) \right] \tag{33}$$

$$u_x = \cos(\alpha - \varphi) \; c_{planar} \int_t \int_t (k_h - k_y) \; dt \, dt$$
$$c_{planar} = g \left[\cos(\alpha - \varphi^*) - \lambda \sin(\alpha - \varphi^*) \right] \tag{34}$$

Numerical methods can be used in the algorithm presented in Fig. 6 to calculate permanent displacement. It should be noted that identical solutions have been obtained by closed-form analytical formulations derived in the framework of limit equilibrium in previous studies (e.g., Ghanbari *et al.* 2013).
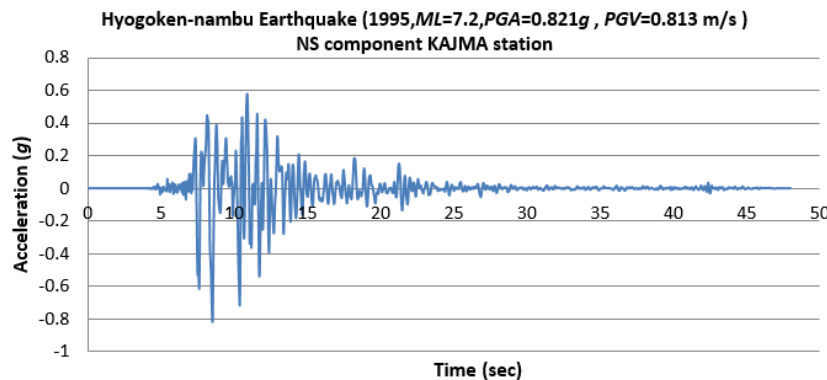

Fig. 8 Hyogoken-Nambu earthquake record (http://peer.berkeley.edu/smcat/search.html)

H=10 m, ϕ^*=30°, c*=0, β=60°, γ=18 kN/m³, b=6 m, k_t/γh=0.3, λ=0.2

(a)

H=10 m, ϕ^*=30°, c*=0, β=60°, γ=18 kN/m³, b=6 m, k_t/γh=0.3, λ=0.2


(b)
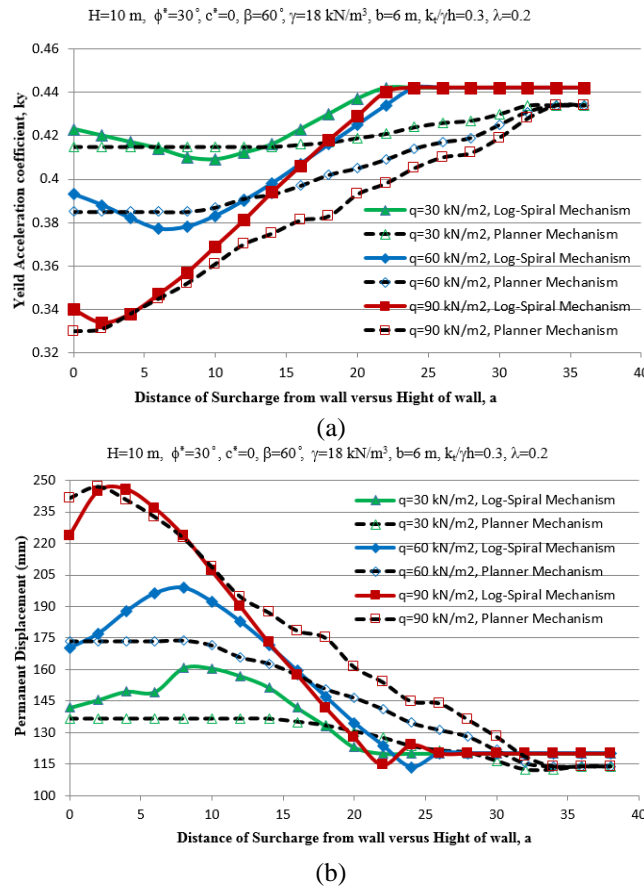
Fig. 9 Variations of (a) yield acceleration and (b) displacement of slope versus the distance of surcharge from the end of the slope for different intensities of surcharge

5. The results of the suggested method

Variations of yield acceleration versus distance of surcharge from the edge of slope for different widths are shown in Fig. 7(a). As can be observed in this figure, by increasing the distance of surcharge, the yield acceleration becomes critical for the log-spiral rotational case due to an increase in the rotational moment of the surcharge. As the distance of surcharge from the edge of the slope is increased again, the effect of surcharge is decreased and the planar condition becomes critical. In this figure, the height of the center of mass of the building is 8 m. In this formulation, k_y=0 means the slope is at static equilibrium and values of k_y<0 are relevant to unstable slopes.

In Fig. 7(b), variations of the displacement of the slope for different distances and widths of the surcharge for Hyogoken-nambu-1995 earthquake (Fig. 8) have been studied. As can be observed in this figure, for the shorter distances of surcharge from the edge of the slope the displacements are greater in the rotational case. Eventually, as the surcharge moves to outside of the failure wedge, the displacements become greater in rotational case. In this case, the value of $r_h \sin \theta_h c_{log-spiral}$ is greater than $\cos(\alpha-\varphi) c_{planar}$ which causes an increase in displacements in the rotational case.

H=10 m, φ*=30°, c*=0, γ=18 kN/m³, kₜ/γh=0.3 , q=60 kN/m², b=6 m, hq=18 m, λ=0.2

(a)

H=10 m, φ*=30°, c*=0, γ=18 kN/m³, kt/γh=0.3 , q=60 kN/m², b=6 m, hq=18 m, λ=0.2


(b)
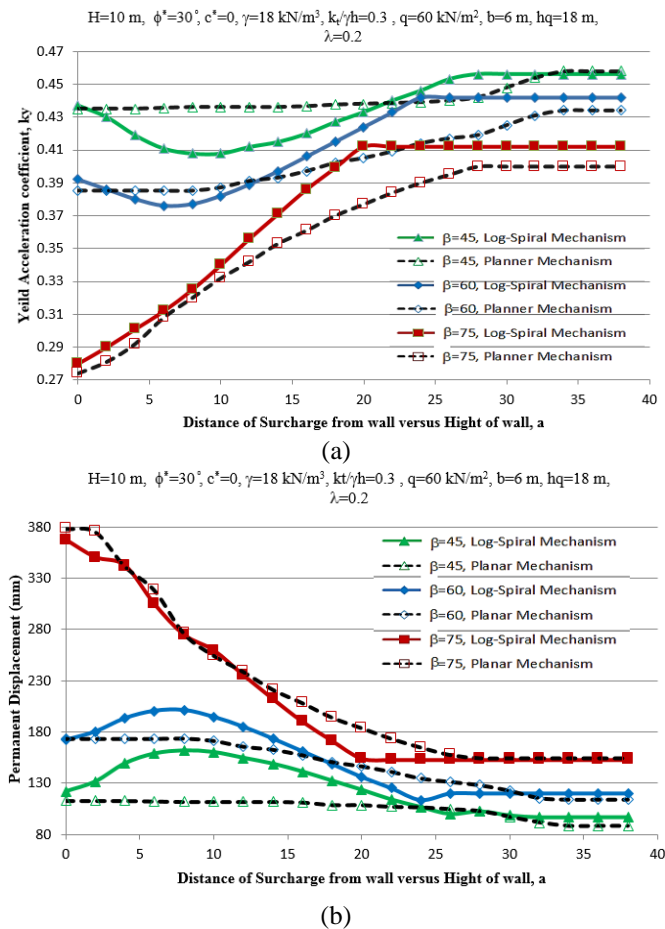
Fig. 10 Variations of (a) yield acceleration and (b) displacement of slope for various angles of slope versus the distance of surcharge from the end of slope

Variations of the yield acceleration and displacement of slope for different intensity and distance of surcharge are shown in Fig. 9. As can be observed in this figure, by increase in the intensity of surcharge, the acceleration is decreased and the displacement is increased. By increasing the distance of the surcharge from the slope, the surcharge effect finally disappeared and the slope performed as the case without the surcharge. The height of the building is obtained with regard to the specific weight of the whole building (3.33 kN/m³).

Fig. 10 shows variations of the yield acceleration and displacement of the slopes with different angles and various distances of surcharge. The steeper slopes show smaller yield accelerations and larger displacements.

6. Comparison between the results

Among the studies reported by other researchers, the effect of surcharge on yield acceleration and displacement of slopes has rarely been evaluated. A comparison is presented here between the

previous works and the results of the method suggested in this paper for the case without a surcharge and associated flow rule.

Table 1 shows a comparison between the results of the suggested formulation in transitional mode and the results reported by Ausilio *et al.* (2000) and Ling *et al.* (1997). Also, Table 2 shows a comparison between the results of the suggested formulation with those of Ausilio *et al.* (2000) in transitional and rotational modes. The results show a good agreement between the suggested method and the previously reported data. The results of the suggested method are compared in Table 3 with those of Michalowski and You (2000) for a case without a surcharge in rotational mode. A good agreement between the results can be observed for this case too.

Table 1 Comparison of k_y values form suggested method, Ausilio *et al.* (2000) and Ling *et al.* (1998)

	Amagasaki wall	Gould wall	Valencia wall	Seiken wall
H (m)	4.7	4.6	6.4	5.5
β (degrees)	90	86.4	86.4	78.7
ϕ (degrees)	35	33	33	37
γ (kN/m^3)	20	20	20	18
T_u (kN/m^3)	38	36	36	20
k_y proposed method	0.271	0.302	0.301	0.385
k_y Ausilio *et al.* (2000)	0.306	0.310	0.322	0.415
k_y Ling *et al.* (1997)	0.310	0.312	0.324	0.427

Table 2 Comparison of k_y values from suggested method and Ausilio *et al.* (2000) for the rotational and transitional case

$H=L$=5 m, γ =18 kN/m^3,C =0 kN/m^2, λ =0, q=0 kN/m^2						
ϕ (degrees)	β (degrees)	k_t	k_y (log-spiral mechanism)		k_y (planar mechanism)	
			Proposed method	Ausilio *et al.* (2000)	Proposed method	Ausilio *et al.* (2000)
30	60	24.75	0.436	0.450	0.430	0.430
40	60	24.75	0.650	0.640	0.615	0.610
30	60	15.75	0.308	0.320	0.303	0.300
30	45	24.75	0.476	0.485	0.469	0.480
40	45	24.75	0.369	0.380	0.372	0.380

Table 3 Comparison of k_y values from suggested method and Michalowski and You (2000)

ϕ (degrees)	β (degrees)	$k_t/\gamma H$	k_y (log-spiral mechanism)	
			Proposed method	Michalowski and You (2000)
30	60	0.3	0.441	0.442
30	45	0.3	0.458	0.465
30	75	0.3	0.401	0.400
40	60	0.2	0.504	0.510
40	50	0.4	0.737	0.740

Table 4 Comparison of k_y values from suggested method and Michalowski (2007)

H= 5 m, γ=18 kN/m^3, ϕ=28°, C =10.8 kPa, λ=0, q=0 kN/m^2, k_t=0			
k_y (Proposed method)		k_y (Michalowski 2007)	
Log-spiral mechanism	Planar mechanism	Log-spiral mechanism	Planar mechanism
0.241	0.308	0.240	0.310

Table 5 Comparison of the displacement value from suggested method and Michalowski (2007)

H= 5 m, γ=18 kN/m^3, ϕ=28°, C =10.8 kPa, λ=0, q=0 kN/m^2, k_t=0			
Displacement (mm) (Proposed method)		Displacement (mm) (Michalowski 2007)	
Log-spiral mechanism	Planar mechanism	Log-spiral mechanism	Planar mechanism
42.96	3.91	43.00	3.60

Tables 4 and 5 show a comparison between the coefficient of yield acceleration and displacement of the slope obtained from the suggested method in this research and the method of Michalowski (2007) for a case without a surcharge. The displacements are obtained for the Loma Prieta Earthquake-1989, California Strong Motion Instrumentation Program (CSMIP) station No. 57007, magnitude 7.1, direction 90°, peak acceleration 469 cm/s^2, distance to epicenter 5 km (http://peer.berkeley.edu/smcat/search.html). As can be observed, the results of the two methods are in good agreement. The comparisons presented in this section confirm the validity of the formulation for the case without a surcharge and the reliability of the formulation in vicinity of a surcharge.

7. Conclusions

Using the non-associated upper bound theory of limit analysis a new formulation is presented in this research for calculating permanent displacements and yield acceleration of reinforced soil slopes in vicinity of a surcharge.

For this purpose, two failure modes, transitional and rotational, have been considered and the results obtained from the two techniques have been compared with each other. In this method, the effect of intensity, width, height and location of surcharge related to the edge of the slope as well as soil properties such as internal friction angle of soil, cohesion and specific weight of soil have been investigated.

The results obtained from the suggested method show the important effect of surcharge on displacements of the slope. For the case where the surcharge has a small distance from the edge of the slope, it is possible that the rotational mode would result in greater displacements compared to the transitional model. The reason is an increase in the arm of the moment induced by surcharge. As the distance of the surcharge from the edge of the slope is increased and thus the effect of surcharge is decreased, the transitional mode results in greater displacements. Finally, by increasing the distance of surcharge from the edge of the slope the effect of surcharge disappears and the slope would behave similar to the case without a surcharge. An increase in the intensity or the width of surcharge causes a decrease in yield acceleration and increase in the displacement of slope.

References

Aminpoor, M.M. and Ghanbari, A. (2014), "Design charts for yield acceleration and seismic displacement of retaining walls with surcharge through limit analysis", *Struct. Eng. Mech.*, **52**(6), 1225-1256.

Ausilio, E., Conte, E. and Dente, G. (2000), "Seismic stability analysis of reinforced slopes", *Soil Dyn. Earthq. Eng.*, **19**(3), 159-172.

Askari, F. and Farzaneh, O. (2003), "Upper-bound solution for seismic bearing capacity of shallow foundations near slopes", *Geotechniq.*, **53**(8), 697-702.

Bathurst, R.J., Nernheim, A., Walters, D.L., Allen, T.M., Burgess, P. and Saunders, D.D. (2009), "Influence of reinforcement stiffness and compaction on the performance of four geosynthetic-reinforced soil walls", *Geosynth. Int.*, **16**(1), 43-59.

Bathurst, R.J., Hatami, K. and Alfaro, M.C. (2012), *Geosynthetic Reinforced Soil Walls and Slopes-Seismic Aspects*, *Handbook of Geosynthetic Engineering*, ICE Publishing, London, U.K.

Cai, Z. and Bathurst, R.J. (1996), "Seismic induced permanent displacement of geosynthetic reinforced segmental retaining walls", *Can. Geotech. J.*, **33**(6), 937-955.

Caltabiano, S., Cascone, E. and Maugeri, M. (2005), "A procedure for seismic design of retaining walls, seismic prevention of damage: A case study in a mediterranean city", *WIT Trans. State Art Sci. Eng.*, **8**, 263-277.

Caltabiano, S., Cascone, E. and Maugeri, M. (2012), "Static and seismic limit equilibrium analysis of sliding retaining walls under different surcharge conditions", *Soil Dyn. Earthq. Eng.*, **37**, 38-55.

Chen, W.F. (2008), *Limit Analysis and Soil Plasticity*, J. Ross Pub.

Crespellani, T., Madai, C. and Vannucchi, G. (1998), "Earthquake destructiveness potential factor and slope stability", *Geotechniq.*, **48**(3), 411-419.

Davis, E.H. (1968), *Theories of Plasticity and Failure of Soil Masses. In Soil Mechanics: Selected Topics,* Elsevier, New York, U.S.A.

El-Emam, M.M. and Bathurst, R.J. (2005), "Facing contribution to seismic response of reduced-scale reinforced soil walls", *Geosynth. Int.*, **12**(3), 215-238.

El-Emam, M.M. and Bathurst, R.J. (2007), "Influence of reinforcement parameters on the seismic response of reduced-scale reinforced soil retaining walls", *Geotext. Geomembr.*, **25**(1), 33-49.

Fei, Z., Yufeng, G., Yongxin, W., Ning, Z. and Yue, Q. (2016), "Effects of vertical seismic acceleration on 3D slope stability," *Earthq. Eng. Eng. Vibr.*, **15**(3), 487-494.

Ghanbari, A. and Taheri, M. (2012), "An analytical method for calculating active earth pressure in reinforced retaining walls subject to a line surcharge", *Geotext. Geomembr.*, **34**, 1-10.

Ghanbari, A., Khalilpasha, A., Sabermahani, M. and Heydari, B. (2013), "An analytical technique for estimation of seismic displacements in reinforced slopes based on horizontal slices method (HSM)", *Geomech. Eng.*, **5**(2),143-164.

Huang, C.C. and Wang, W.C. (2005), "Seismic displacement charts for the performance-based assessment of reinforced soil walls", *Geosynth. Int.*, **12**(4), 176-190.

Huang, C.C. and Wu, S.H. (2006), "Simplified approach for assessing seismic displacements of soil-retaining walls. Part I: Geosynthetic reinforced modular block walls", *Geosynth. Int.*, **13**(6), 219-233.

Huang, C.C. and Wu, S.H. (2007), "Simplified approach for assessing seismic displacements of soil-retaining walls. Part II: Geosynthetic-reinforced walls with rigid panel facing", *Geosynth. Int.*, **14**(5), 264-276.

Huang, C.C., Horng, J.C. and Charng, J.J. (2008), "Seismic stability of reinforced slopes: Effects of reinforcement properties and facing rigidity", *Geosynth. Int.*, **15**(2), 107-118.

Huang, C.C. and Wu, H.J. (2009), "Seismic displacement analyses for a reinforced soil wall considering progressive development of reinforcement force", *Geosynth. Int.*, **16**(3), 222-234.

Huang, C.C. and Luo, W.M. (2010), "Behavior of cantilever and geosynthetic-reinforced walls on deformable foundations", *Geotext. Geomembr.*, **28**(5), 448-459.

Huang, C.C., Horng, J.C., Chang, W.J. and Chiou, J.S. (2011), "Dynamic behavior of reinforced walls-

Horizontal displacement response", *Geotext. Geomembr.*, **29**(3), 257-267.

Krishna, A.M. and Latha, G.M. (2009), "Seismic behaviour of rigid-faced reinforced soil retaining wall models: reinforcement effect", *Geosynth. Int.*, **16**(5), 364-373.

Lee, K.Z.Z., Chang, N.Y. and Ko, H.Y. (2010), "Numerical simulation of geosynthetic-reinforced soil walls under seismic shaking", *Geotext. Geomembr.*, **28**(4), 317-334.

Liang, T., Shengyi, C., Xianzhang, L. and Nengpan, J. (2017), "The boundary conditions for simulations of ashake-table experiment on the seismic response of 3D slope," *Earthq. Eng. Eng. Vibr.*, **16**(1), 23-32.

Liu, H. (2009), "Analyzing the reinforcement loads of geosynthetic-reinforced soil walls subject to seismic loading during the service life", *J. Perform. Constr. Fac.*, **23**(5), 292-302.

Liu, H., Wang, X. and Song, E. (2011), "Reinforcement load and deformation mode of geosynthetic-reinforced soil walls subject to seismic loading during service life", *Geotext. Geomembr.*, **29**(1), 1-16.

Michalowski, R.L. (1998), "Limit analysis in stability calculations of reinforced soil structures", *Geotext. Geomembr.*, **16**(6), 311-331.

Michalowski, R.L. and You, L. (2000), "Displacements of reinforced slopes subjected to seismic loads", *J. Geotech. Geoenviron. Eng.*, **126**(8), 685-694.

Michalowski, R.L. (2007), "Displacement of multiblock geotechnical structures subjected to seismic excitation", *J. Geotech. Geoenviron. Eng.*, **133**(11), 1432-1439.

Mojallal, M. and Ghanbari, A. (2012), "Prediction of seismic displacements in gravity retaining walls based on limit analysis approach", *Struct. Eng. Mech.*, **42**(2), 247-267.

Mojallal, M., Ghanbari, A. and Askari, F. (2012), "A new analytical method for calculating seismic displacements in reinforced retaining walls", *Geosynth. Int.*, **19**(3), 212-231.

Madhavi Latha, G. and Murali Krishna, A. (2008), "Seismic response of reinforced soil retaining wall models: Influence of backfill relative density", *Geotext. Geomembr.*, **26**(4), 335-349.

Sloan, S.W. (2013), "Geotechnical stability analysis", *Geotechniq.*, **63**(7), 531-572.

Srilatha, N., Madhavi Latha, G. and Puttappa, C.G. (2013), "Effect of frequency on seismic response of reinforced soil slopes in shaking table tests", *Geotext. Geomembr.*, **36**, 27-32.

Tatsuoka, F., Hirakawa, D., Nojiri, M., Aizawa, H., Nishikiori, H., Soma, R., Tateyama, M. and Watanabe, K. (2009), "A new type of integral bridge comprising geosynthetic-reinforced soil walls", *Geosynth. Int.*, **16**(4), 301-326.

Varzaghani, M I. and Ghanbari, A. (2014), "A new analytical model to determine dynamic displacement of foundations adjacent to slope", *Geomech. Eng.*, **6**(6), 103-121.

Yang, G., Zhang, B., Lv, P. and Zhou, Q. (2009), "Behaviour of geogrid reinforced soil retaining wall with concrete-rigid facing", *Geotext. Geomembr.*, **27**(5), 350-356.

Yu, S.B., Merifield, R.S., Lyamin, A.V. and Fu, X.D. (2014), "Kinematic limit analysis of pullout capacity for plate anchors in sandy slopes", *Struct. Eng. Mech.*, **51**(4), 565-579.

Zhang, G., Tan, J., Zhang, L. and Xiang, Y. (2016), "Limit analysis of 3D rock slope stability with non-linear failure criterion", *Geomech. Eng.*, **10**(1), 59-76.

CC

Appendix

The functions f_1 to f_6 are defined as following (Crespellani *et al.* 1998, Michalowski 1998), in this paper, φ^* must be used instead of φ.

$$f_1(\theta_0, \theta_h) = \frac{\{(3 \tan \varphi \cos \theta_h + \sin \theta_h) \exp[3(\theta_h - \theta_0) \tan \varphi] - 3 \tan \varphi \cos \theta_0 - \sin \theta_0\}}{3(1 + 9 \tan^2 \varphi)} \tag{35}$$

$$f_2(\theta_0, \theta_h) = \frac{1}{6} \frac{X}{r_0} \left(2 \cos \theta_0 - \frac{X}{r_0}\right) \sin \theta_0 \tag{36}$$

$$f_3 = \frac{1}{6} \exp[(\theta_h - \theta_0) \tan \varphi] \left[\sin(\theta_h - \theta_0) - \frac{X}{r_0} \sin \theta_h\right] \times \left\{\cos \theta_0 - \frac{X}{r_0} + \cos \theta_h \exp[(\theta_h - \theta_0) \tan \varphi]\right\} \tag{37}$$

$$f_4(\theta_0, \theta_h) = \frac{1}{3(1 + 9 \tan^2 \varphi)} \{(3 \tan \varphi \sin \theta_h - \cos \theta_h) \exp[3(\theta_h - \theta_0) \tan \varphi] - 3 \tan \varphi \sin \theta_0 + \cos \theta_0\} \tag{38}$$

$$f_5(\theta_0, \theta_h) = \frac{1}{3} \frac{X}{r_0} \sin^2 \theta_0 \tag{39}$$

$$f_6(\theta_0, \theta_h) = \frac{1}{6} \exp[(\theta_h - \theta_0) \tan \varphi] \left[\sin(\theta_h - \theta_0) - \frac{X}{r_0} \sin \theta_h\right] \times \{\sin \theta_0 + \sin \theta_h \exp[(\theta_h - \theta_0) \tan \varphi]\} \tag{40}$$

$$\frac{X}{r_0} = \frac{1}{\sin \theta_h} \left[\sin(\theta_h - \theta_0) - \frac{H}{r_0} \frac{\sin(\beta + \theta_h)}{\sin \beta}\right] \tag{41}$$

$$\frac{H}{r_0} = \sin \theta_h \exp[(\theta_h - \theta_0) \tan \varphi] - \sin \theta_0 \tag{42}$$

The moment of inertia for the soil mass failed by rotational mechanism, defined as following

$$I_{OBC} = \int_{\theta_0}^{\theta_h} \frac{1}{2} \rho r^4 d\theta = \frac{1}{2} \rho r_0^4 \int_{\theta_0}^{\theta_h} \exp[4(\theta - \theta_0) \tan \varphi] d\theta$$
$$= \frac{1}{8} \rho r_0^4 \frac{1}{\tan \varphi} \{\exp[4(\theta_h - \theta_0) \tan \varphi] - 1\} \tag{43}$$